

## Progress in piezo-phototronic effect modulated photovoltaics

This content has been downloaded from IOPscience. Please scroll down to see the full text.

2016 J. Phys.: Condens. Matter 28 433001

(<http://iopscience.iop.org/0953-8984/28/43/433001>)

View [the table of contents for this issue](#), or go to the [journal homepage](#) for more

Download details:

IP Address: 59.66.211.61

This content was downloaded on 08/09/2016 at 02:27

Please note that [terms and conditions apply](#).

## Topical Review

# Progress in piezo-phototronic effect modulated photovoltaics

Miaoling Que, Ranran Zhou, Xiandi Wang, Zuqing Yuan, Guofeng Hu and Caofeng Pan

Beijing Institute of Nanoenergy and Nanosystems, Chinese Academy of Sciences, National Center for Nanoscience and Technology (NCNST), Beijing 100083, People's Republic of China

E-mail: [cfpan@binn.cas.cn](mailto:cfpan@binn.cas.cn)

Received 5 June 2016, revised 19 July 2016

Accepted for publication 3 August 2016

Published 7 September 2016



## Abstract

Wurtzite structured materials, like ZnO, GaN, CdS, and InN, simultaneously possess semiconductor and piezoelectric properties. The inner-crystal piezopotential induced by external strain can effectively tune/control the carrier generation, transport and separation/combination processes at the metal-semiconductor contact or p–n junction, which is called the *piezo-phototronic effect*. This effect can efficiently enhance the performance of photovoltaic devices based on piezoelectric semiconductor materials by utilizing the piezo-polarization charges at the junction induced by straining, which can modulate the energy band of the piezoelectric material and then accelerate or prevent the separation process of the photon-generated electrons and vacancies. This paper introduces the fundamental physics principles of the *piezo-phototronic effect*, and reviews recent progress in *piezo-phototronic effect* enhanced solar cells, including solar cells based on semiconductor nanowire, organic/inorganic materials, quantum dots, and perovskite. The *piezo-phototronic effect* is suggested as a suitable basis for the development of an innovative method to enhance the performance of solar cells based on piezoelectric semiconductors by applied extrinsic strains, which might be appropriate for fundamental research and potential applications in various areas of optoelectronics.

Keywords: the piezo-phototronic effect, photovoltaics, wurtzite structured semiconductors, ZnO, GaN, CdS, and InN, piezo-polarization charges

(Some figures may appear in colour only in the online journal)

## 1. Introduction

Micro/nano electronic systems, composed of micro/nano transistors, supercapacitors, photoelectric switches, and light emitting diodes (LED), etc, play an essential role in advancing the internet of things [1–3], smart city building [4, 5] and robot technology [6, 7]. Nanomaterial and nanostructure based miniaturized solar cells, a promising energy supply for such micro/nano systems, have been broadly researched [8–10]. Conventional approaches to enhance the solar cells performance, such as introducing highly efficient energy materials and improving device structures, have been researched

adequately up to now [11, 12]. The open circuit voltage of a solar cell can be optimized by modulating the thickness of the p–n junction according to the thermodynamic theory [13, 14]. In silicon solar cells, metal-insulator-semiconductor (MIS) structures instead of p–n junctions have been applied to reduce the saturation current density of the device [15, 16]. From a materials point of view, polymers with small band gap have been utilized to improve the open circuit voltage of polymer solar cells [17]. In addition, perovskite solar cells have emerged as a promising candidate for higher energy conversion efficiency due to their excellent optical characteristics [18–20]. Recently, a brand new method has been proposed as

very effective in enhancing the performance of solar cells by using piezoelectronic materials [21, 22], which has already attracted extensive concern.

Typical piezoelectric semiconducting materials (such as ZnO, CdS, GaN and InN) will create a piezoelectric potential inside the crystal under external strain, due to their non-central symmetric wurtzite structure [23, 24]. The *piezo-phototronic effect*, which is utilizing the inner-crystal piezopotential as a ‘gate’ voltage to tune/control the charge generation, separation, transportation and/or recombination in the local interface area [25], has already been used to enhance the light emitting efficiency of LEDs [26–28], improve the sensitivity of photo-detectors [29, 30], and enhance charge separation of the solar cells or photocells [31, 32]. Combined with the *piezo-phototronic effect*, solar cells can not only capture solar energy, but are also able to collect mechanical energy from the surrounding environment, which indicates their prospective potential for application in micro/nano smart sensor networks [33].

In this article, we have reviewed the recent research progress in *piezo-phototronic effect* enhanced solar cells. First, the fundamental physics of the *piezo-phototronic effect* is elaborated, and the working principles to optimize the performance of solar cells are explored. Then a wide range of piezoelectric micro/nanomaterial based solar cells with elevated performance tuned by the *piezo-phototronic effect* are presented. Finally, a brief summary and some future prospects for the *piezo-phototronic effect* enhanced solar cells are given.

## 2. Fundamental physics of piezo-phototronics

### 2.1. Piezoelectric polarization

For wurtzite-structured piezoelectric semiconductor materials, strain induced piezoelectric polarization charges (piezo-charges) will distribute at the two ends of the crystal along a specific orientation [34–36]. Taking ZnO as an example, which has a hexagonal structure and possesses anisotropic properties both along and perpendicular to the  $c$ -axis direction, the  $\text{Zn}^{2+}$  cations and  $\text{O}^{2-}$  anions are tetrahedrally coordinated [37], and their charge centers are overlapped with each other. If the crystal is subjected to stress along the  $c$ -axis, there will be a displacement between the cation center and the anion center, inducing an electrical dipole moment as shown in figure 1(a) [38]. All the dipole moments within the crystal will accumulate and result in a macroscopic electric potential difference along the direction of applied strain in the crystal, which is called the piezopotential, short for piezoelectric potential. Figure 1(b) shows that the negative and positive piezo-charges appear in the  $+c$  and  $-c$  direction respectively under compressive strain [39]. If the applied stress changes to effect a tensile strain, the piezopotential reverses, and the aligned ZnO nanowire (NW) arrays are shown in figure 1(c) [40]. Herein, piezopotential, a strain-induced inner-crystal field, is the crucial fundament for the emergence of *piezotronics* and *piezo-phototronics*, which allows modulation of the carrier transport properties at the M–S interface or p–n junction and thus effectively tunes/controls the performance of the electronic devices.

### 2.2. Piezoelectric polarization at metal–semiconductor (M–S) contact

The M–S contact, formed by contacting metal with semiconductors, is an important foundation for electronics and optoelectronics based on semiconductors [41]. At the interface area of M–S contact, a significant redistribution of charges occurs and the fermi levels on both sides of the interface must be aligned to reach the thermal equilibrium of the system. This results in energy band deformation in the semiconductor near the M–S junction and consequently in forming an energy barrier at the local M–S interface, where the barrier height is defined as  $e\Phi_{\text{Bn}}$ , which is called the Schottky barrier height (SBH). The SBH is an evaluation of the energy level mismatch at the M–S interface, which dominates the majority carrier transport process in this area [42, 43].

If the semiconductor material in a M–S contact possesses the piezoelectric property, taking an n-type semiconductor for example and ignoring the surface states and other defects for simplification, the negative piezo-charges induced by compressive strain will distribute at the junction interface along the  $+c$  axis of the semiconductor, which can repel the electrons away from the interface and thus create a wider depletion region and a higher local SBH (figure 2(a)) [44, 45]. In contrast, the tensile-strain-induced positive piezo-charges at the interface along the  $+c$  axis will attract electrons, resulting in a narrower depletion region and hence a lower local SBH (figure 2(b)) [46].

According to the diffusion theory, majority carriers dominate the carrier transportation in a M–S contact, and under the forward bias, the current density ( $J_n$ ) can be expressed as [43]:

$$J_n \approx J_D \cdot \left[ \exp\left(\frac{qV}{kT}\right) - 1 \right] \quad (1)$$

$$J_D \approx q^2 D_n N_c \cdot (kT)^{-1} \sqrt{[2qN_D(\Psi_{\text{bi}} - V)\varepsilon_s^{-1}]} \left( \exp\frac{-q\Phi_{\text{Bn}}}{kT} \right) \quad (2)$$

Here,  $J_D$  represents the saturation current density,  $\varepsilon_s$  depicts the permittivity of the semiconductor material,  $D_n$  is the electron diffusion coefficient,  $N_c$  is the effective states density in the conduction band, and  $N_D$  is the donor concentration in the semiconductor. While under the situation of no piezoelectric polarization charge, the saturation current density ( $J_{D0}$ ) can be defined as:

$$J_{D0} \approx q^2 D_n N_c (kT)^{-1} \sqrt{[2qN_D(\Psi_{\text{bi}0} - V)\varepsilon_s^{-1}]} \left[ \exp\frac{-q\Phi_{\text{Bn}0}}{kT} \right] \quad (3)$$

where  $\Psi_{\text{bi}0}$  represents the built-in potential. When the semiconductor is subjected to a strain, the piezo-charges created at the local interface will not only change the SBH, but also the width of the barrier. The changed SBH is then derived as  $\Phi_{\text{Bn}} = \Phi_{\text{Bn}0} - q^2 \rho_{\text{piezo}} W_{\text{piezo}}^2 (2\varepsilon_s)^{-1}$ , where  $W_{\text{piezo}}$  is the thickness of the piezoelectric polarization charge layer, which distributes in the M–S interface area and is assumed much smaller than the width of the charge depletion region.  $\rho_{\text{piezo}}$  represents the density of created piezo-charges. Then the current density flowing through the barrier can hence be derived as:

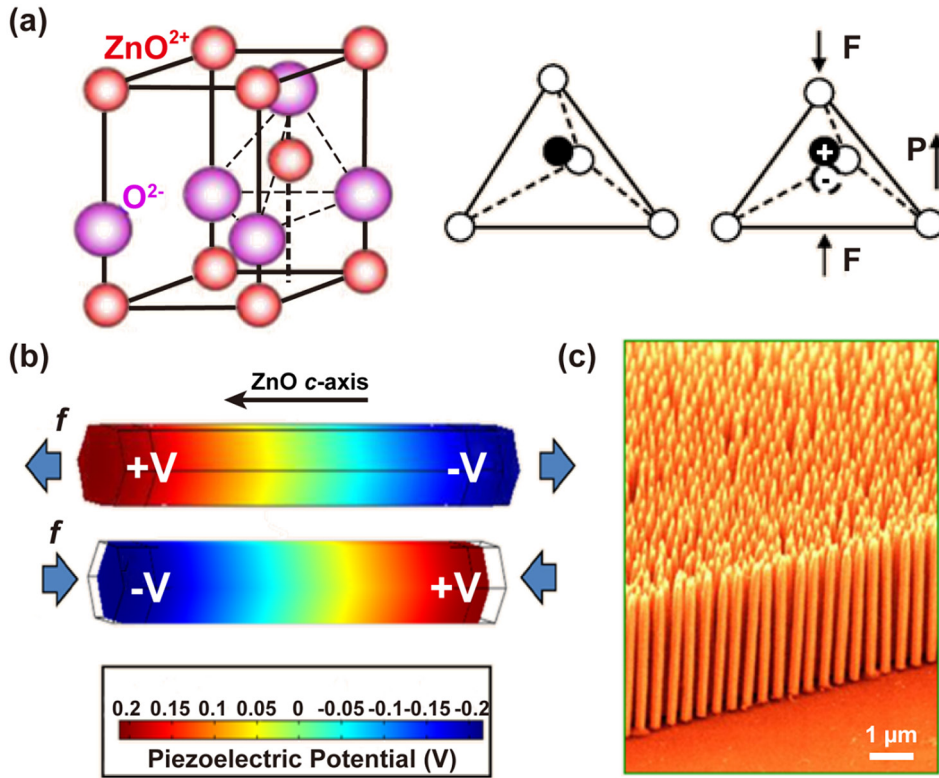


**Figure 1.** Piezopotential in wurtzite-structured crystal. (a) Atomic model of the wurtzite-structured ZnO crystal. (b) Numerical calculated piezopotential distribution along a ZnO NW under axial strain. Reproduced with permission [39]. Copyright 2009. AIP. (c) Aligned ZnO nanowire arrays synthesized by solution process. (a) and (c) Reproduced with permission [38]. Copyright 2012, Wiley-VCH.

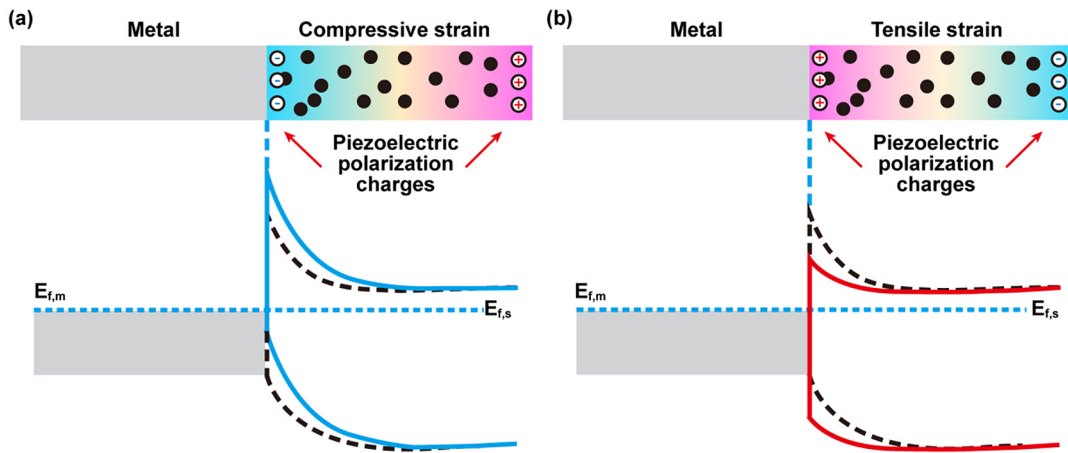


**Figure 2.** Schematic of energy band diagram illustrating the piezoelectric effect on the interface of metal–semiconductor contact. (a) Compressive strain induced negative piezo-charges near the interface, increasing the local SBH (the raised blue solid curves). (b) Tensile strain induced positive piezo-charges near the interface, decreasing the local SBH (the declining red solid curves). The color gradients illustrate the distribution of piezopotential, red represents positive piezopotential and blue represents negative piezopotential. (a) and (b) Reproduced with permission [38]. Copyright 2012, Wiley-VCH.

$$J_n \approx J_{D0} \cdot \exp \left[ q^2 \rho_{\text{piezo}} W_{\text{piezo}}^2 (2kT\varepsilon_s)^{-1} \right] \cdot \exp \left( \frac{qV}{kT} - 1 \right) \quad (4)$$

A more specific correlation between the applied strain and SBH can be defined as:

$$P_Z = e_{33}s_{33} = q\rho_{\text{piezo}}W_{\text{piezo}} \quad (5)$$

$e_{33}$  represents the piezoelectric coefficient,  $s_{33}$  is the induced strain along the polar axis of the piezoelectric semiconductor

material. Ultimately, the current density through the Schottky barrier can be expressed as:

$$J \approx J_{D0} \cdot \exp \left[ qe_{33}s_{33}W_{\text{piezo}} \cdot (2kT\varepsilon_s)^{-1} \right] \cdot \exp \left( \frac{qV}{kT} - 1 \right) \quad (6)$$

This equation apparently indicates that the polarity of the induced strain affects the current transportation across the M–S interface directly. When compressive strain induced negative piezo-charges (negative  $\rho_{\text{piezo}}$  and thus negative  $s_{33}$ ) are

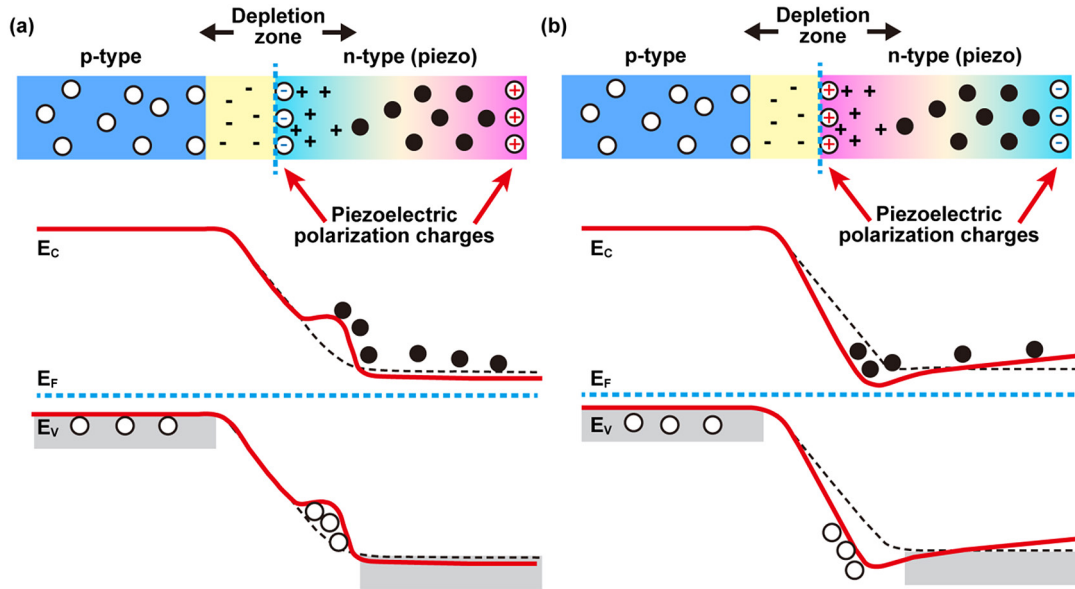


**Figure 3.** Schematic of energy band diagram depicting the piezoelectric effect on the p–n homojunction. The strain induced piezo-charges near the junction interface result in the deformation of energy band at the contact, shown as the red solid curves. The color gradients illustrate the distribution of piezopotential, red represents positive piezopotential and blue represents negative piezopotential. (a) and (b) Reproduced with permission [38]. Copyright 2012, Wiley-VCH.

introduced to the local M–S contact, the current density will decrease correspondingly. Conversely, when the induced strain is switched to a tensile strain, the transport current density will increase. In the former circumstance, there is a prominent rise in the SBH; in the latter a reduction. This is the fundamental mechanism that illustrates how the piezo-polarization charges modulate the carrier transport properties cross the M–S contact.

### 2.3. Piezoelectric polarization at the p–n junction

Apart from M–S contact, some modern electronics and optoelectronics, such as solar cells [47], LEDs [48] and photodetectors [49], also utilize p–n junctions as their building blocks, where the junction usually consists of a p-type doped and an n-type doped semiconductor material. When the p-type and n-type semiconductors form a junction, the carriers (electrons and holes) adjacent to the junction on both sides will diffuse across the junction and redistribute to balance the local potential and reach thermal equilibrium, thus creating a charge depletion zone and finally forming a built-in electric field. The amount of free carriers in the charge depletion zone is negligible and once the piezo-charges are introduced and preserved in this region, they will significantly modulate the energy band in the local area of the p–n junctions and the carrier transportation as well [35, 50].

For a homogeneous p–n junction, where only the n-type material (ZnO NW grown along *c*-axis) is piezoelectric, when a compressive strain is applied along the *c*-axis, the induced negative piezopotential in the +*c* direction at the junction interface can repel electrons away from the interface, resulting in a shoulder in the local band profile (figure 3(a)) [38]. The inclined energy band will accelerate the electron–hole separation, which would be beneficial and meaningful for solar cell applications. Conversely, the tensile strain induced positive

piezopotential in the local junction interface will attract and accumulate electrons, and result in a decline in the local energy band (figure 3(b)), which will promote electron–hole recombination and improve the performance of LED applications. According to the abrupt junction model, the doping concentration changes abruptly from p-type region to n-type region in a p–n junction. The built-in potential can be expressed as [51]:

$$\Psi_{bi} = \frac{q}{2\epsilon_s} \cdot (N_A W_{Dp}^2 + \rho_{piezo} W_{piezo}^2 + N_D W_{Dn}^2) \quad (7)$$

where  $N_D$  is the donor concentration,  $N_A$  represents the acceptor concentration, and  $W_{Dp}$  and  $W_{Dn}$  represent the width of the depletion region on the p-side and n-side respectively. This equation clearly indicates that the strain-induced piezo-charges can modulate the built-in potential significantly, which is of vital importance in optoelectronic applications. For simplicity, we assume that  $P_{n0} > N_{p0}$ , where  $P_{n0}$  and  $N_{p0}$  represent the hole concentration in the n-type material and the electron concentration in the p-type material, respectively, under thermal equilibrium. The total current density across the p–n junction with the piezopotential is:

$$J = J_{C0} \cdot \exp [q^2 \rho_{piezo} W_{piezo}^2 (2kT\epsilon_s)^{-1}] \cdot \exp [qV \cdot (kT)^{-1} - 1] \quad (8)$$

where  $J_{C0}$  is the saturation current density in the absence of a piezopotential situation. This suggests that the current transported through the junction region has an exponential relation to the piezo-charge density, which is related to the type of strain applied (tensile or compressive).

### 2.4. Piezotronic and piezo-phototronic effect

On the basis of our above presentation, we see that the strain induced piezo-charges regulate the energy band of the

piezoelectric semiconductor close to the junction, which in turn effectively tunes the carrier transport properties. Using the inner crystal potential induced by piezo-charges to control/tune the charge carrier transport characteristics, this is the *piezotronic effect* [40, 52], on the basis of which numerous of mechanical-electronic devices are fabricated. This fundamental theory will support a wide range of potential applications, such as human-computer interfacing, nanorobotics and sensors [53–55].

The nature of the *piezo-phototronic effect* [40] lies in tuning the effect of piezoelectric polarization on the carrier generation, transport, separation or recombination process at the junction interface. It suggests that the performance of optoelectronic devices and interaction with light are significantly changed by externally applied strain, which might have widespread potential applications in solar cells, photodetectors, lasers and LEDs, etc [56, 57].

The piezotronic and piezo-phototronic effect may be influenced by the size of nanostructures due to the size dependence of Young’s modulus in materials. According to previous research, Young’s modulus decreases with the decreasing diameter of NWs, thus resulting in reduced piezotronic and piezo-phototronic effect [58]. In addition, the piezotronic and piezo-phototronic effect will be reduced as temperature increases. This is because the effective piezoelectric polarization surface/interface charges will decrease due to the enhanced screening effect, which results from the increased number of mobile charge carriers in nanostructures at higher temperature [59, 60].

### 3. Theoretical analysis of piezo-phototronic effect on solar cells

The core idea of improving the overall performance of solar cells by including piezoelectric materials is to use the strain-induced potential in the piezoelectric material to promote the separation of photon-generated electron–hole pairs [61]. To further understand the basic theory of the *piezo-phototronic effect* on solar cells, Zhang *et al* proposed the application of analytical mode and theoretical calculations to a typical n-type ZnO NW solar cell based on p–n junction—the p-type material being non-piezoelectric—as shown in figure 4(a) [62]. Upon compressive/tensile strain, the corresponding negative/positive piezopotential significantly modifies the band structure at the interface, which enhances/suppresses the separation of electron–hole pairs, resulting in correspondingly increased/decreased performance of the solar cell as illustrated in figures 4(b) and (c).

To quantitatively analyze the *piezo-phototronic effect* on solar cells, we assume that the generation rates of electrons and holes ( $G_n$  and  $G_p$ ) are constant [63]:

$$G_n = G_p = J_{\text{solar}} \cdot [q(L_n + L_p)]^{-1} \quad (9)$$

where  $J_{\text{solar}}$  is the short circuit current density,  $L_n$  and  $L_p$  represent the electron and hole diffusion lengths respectively. Moreover, we assume that there is no photon emission in our model,  $U_n = U_p = 0$ . For a simplified ideal p–n junction

piezoelectric solar cell, the total current density can be written as:

$$J = J_{\text{pn}} \left[ \exp\left(\frac{qV}{kT}\right) - 1 \right] - J_{\text{solar}}. \quad (10)$$

According to our discussion above,

$$J_{\text{pn}} = J_{\text{pn}0} \cdot \exp [q^2 \rho_{\text{piezo}} W_{\text{piezo}}^2 (2kT\varepsilon_s)^{-1}]. \quad (11)$$

Thus the total current density is derived as:

$$J = J_{\text{pn}0} \cdot \exp [q^2 \rho_{\text{piezo}} W_{\text{piezo}}^2 (2kT\varepsilon_s)^{-1}] \left[ \exp\left(\frac{qV}{kT}\right) - 1 \right] - J_{\text{solar}}. \quad (12)$$

This suggests that the saturation current density  $J_{\text{pn}}$  will decrease exponentially with the piezo-charges generated at the p–n junction interface. It is noted that the sign of the exponential function term in equation (12) reverses, and with it the effect of piezo-potential, under different strain (compressive or tensile). The open circuit voltage ( $V_{\text{oc}}$ ) of the piezoelectric solar cells (PSCs) can be obtained in the situation of  $J = 0$ ,

$$V_{\text{oc}} = \frac{kT}{q} \cdot \ln\left(\frac{J_{\text{solar}}}{J_{\text{pn}}} + 1\right) \quad (13)$$

where  $J_{\text{solar}} \gg J_{\text{pn}}$ ; accordingly the  $V_{\text{oc}}$  can be derived as:

$$V_{\text{oc}} \approx \frac{kT}{q} \cdot \ln\left(\frac{J_{\text{solar}}}{J_{\text{pn}}}\right) = \frac{kT}{q} \cdot \left[ \ln\left(\frac{J_{\text{solar}}}{J_{\text{pn}0}}\right) + q^2 \rho_{\text{piezo}} W_{\text{piezo}}^2 (2kT\varepsilon_s)^{-1} \right]. \quad (14)$$

This indicates that the  $V_{\text{oc}}$  can be modulated by not only the magnitude but also the polarity of the external strain as shown in figure 4(d).

On the other hand, solar cells based on M–S structures are analyzed according to our previous statement about the *piezotronic effect*, in which the semiconductor is n-ZnO nanowire. For simplicity, the total current density across the M–S contact can be written for a PSC:

$$J = J_{\text{MS}} \left[ \exp\left(\frac{qV}{kT}\right) - 1 \right] - J_{\text{solar}} \quad (15)$$

$$J_{\text{MS}} = J_{\text{MS}0} \cdot \exp [q^2 \rho_{\text{piezo}} W_{\text{piezo}}^2 (2kT\varepsilon_s)^{-1}] \quad (16)$$

$$J_{\text{MS}0} \approx q^2 D_n N_c (kT)^{-1} \sqrt{[2qN_D (\Psi_{\text{bi}0} - V) \varepsilon_s^{-1}]} \left[ \exp\left(\frac{-q\Phi_{\text{Bn}0}}{kT}\right) \right] \quad (17)$$

where  $J_{\text{MS}}$  represents the saturation current density in the case with piezo-charges;  $J_{\text{MS}0}$  without.  $\Psi_{\text{bi}0}$  and  $\Phi_{\text{Bn}0}$  are the built-in potential and Schottky barrier height without piezo-charges. Thus, the open circuit voltage of an M–S contact based PSC can be expressed as:

$$V_{\text{oc}} \approx \frac{kT}{q} \cdot \left[ \ln\left(\frac{J_{\text{solar}}}{J_{\text{MS}0}}\right) - q^2 \rho_{\text{piezo}} W_{\text{piezo}}^2 (2kT\varepsilon_s)^{-1} \right]. \quad (18)$$

The equations above suggest that tensile strain induced negative piezo-charges in the interface increase the barrier height

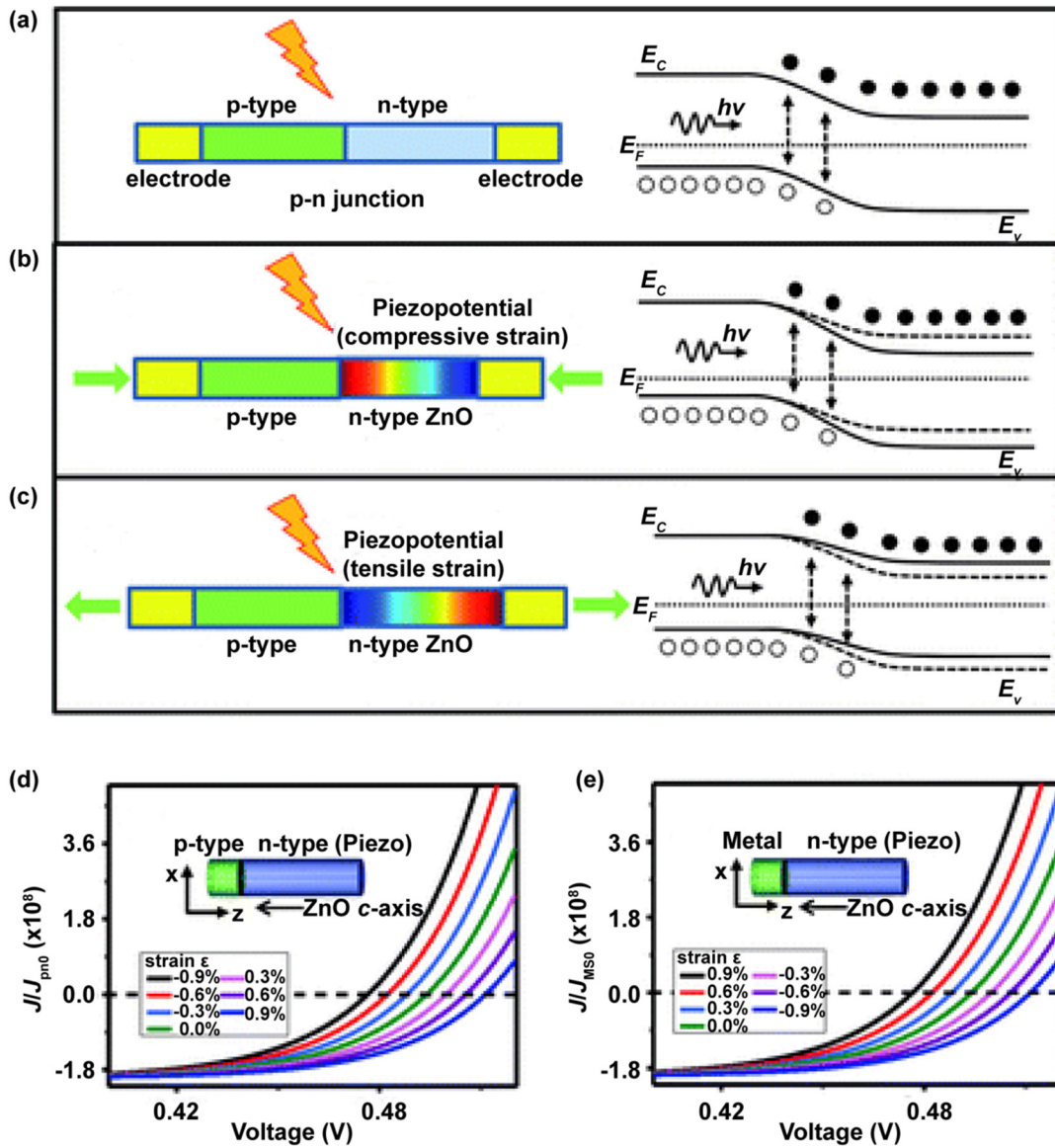


**Figure 4.** Schematic and energy band diagram of a nanowire piezoelectric solar cell based on p–n junction structure (a), under compressive strain (b) and under tensile strain (c). The color gradient represents the piezopotential distribution at the n-type ZnO nanowire. Current-voltage curves of a piezoelectric solar cell based on p–n type (d) and meta-semiconductor (n-ZnO) contact (e) under various applied strains, with the *c*-axis of the piezoelectric n-ZnO nanowire pointing toward the junction. (a)–(e) Reproduced with permission [62]. Copyright 2012, RSC.

of the M–S contact, which decreases the saturation current density  $J_{MS}$  according to equation (17) and increases the open circuit voltage  $V_{oc}$  as shown in equation (18). The opposite phenomena of the  $J$ – $V$  changes under compressive strain can be observed in figure 4(e).

#### 4. Piezo-phototronic effect enhanced performance of semiconductor nanowire solar cells

##### 4.1. Epitaxial strain induced piezoelectric effect in core–shell solar cells

III–V zinc blende (ZB) or III–V wurtzite (WZ) core–shell NWs, consisting of different piezoelectric materials [64], have been researched as a new way to obtain radial p–n junctions. In the epitaxial growth process, the lattice mismatch between

the core and shell materials will introduce an elastic strain in the interface of the core–shell NW, resulting in piezoelectric polarization and thus an internal piezoelectric field along the axis of the NW. According to the fully electroelastically coupled continuum elasticity theory, Xu’s group has studied the analytical model and numerical simulations of the piezoelectric polarization effect in a cylindrical InAs/InP core–shell NW, where the NW is along the [1 1 1] crystallographic orientation, with the length ( $L_z$ ) of 350 nm, the core radius ( $r_c$ ) of 30 nm, and the outer shell radius ( $r_s$ ) of 50 nm. Subsequently, a similar analytical model and numerical simulations of the GaAs/GaP core/shell NW also have been investigated [65].

The numerically computed strain component distributions  $\epsilon_{xx}$  and  $\epsilon_{zz}$  at the  $x$ – $z$  cross section of the ZB InAs/InP core–shell NW are shown in figures 5(a) and (b). The strain component  $\epsilon_{yy}$  is omitted because it is similar to  $\epsilon_{xx}$  with a rotation of

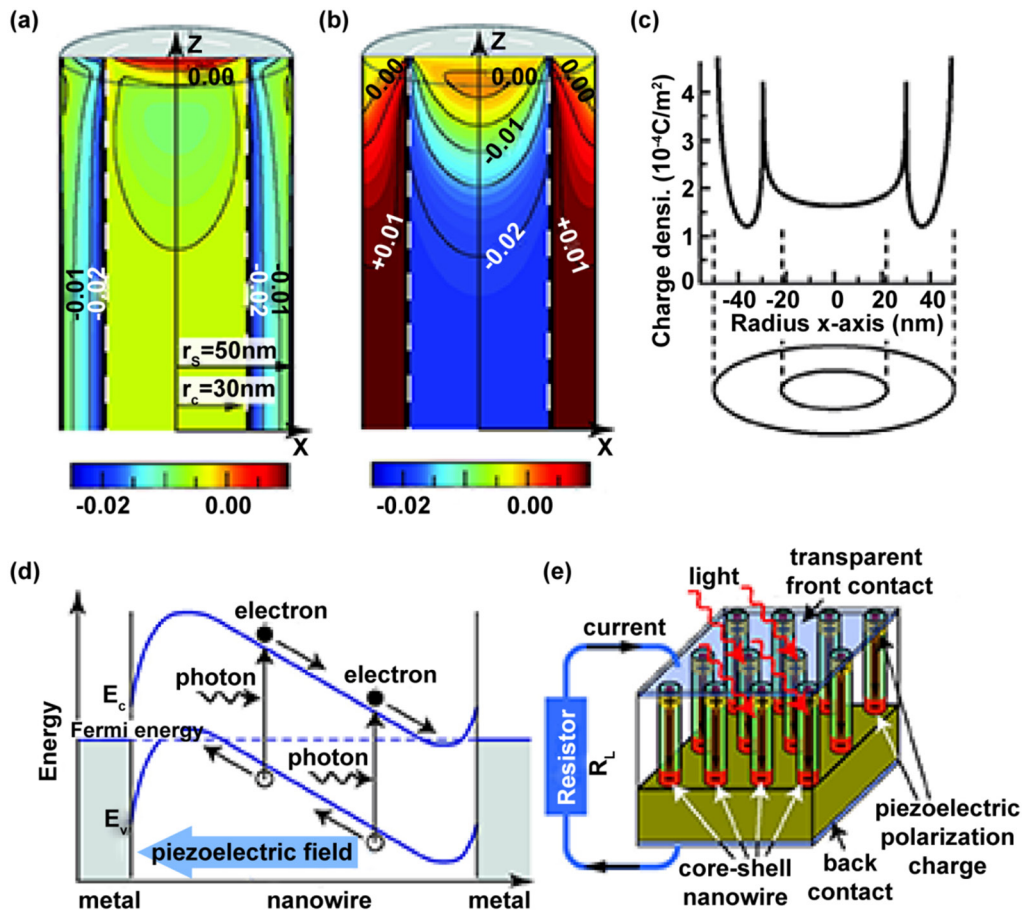


**Figure 5.** Components of strain (a)  $\epsilon_{xx}$  and (b)  $\epsilon_{zz}$  at an  $x$ - $z$  cross section of a cylindrical InAs/InP core-shell NW, which is along the direction of [1 1 1]. (c) Effective surface charge density in InAs/InP WZ core-shell NW in vacuum. (d) Schematic illustration of the band diagram and the photovoltaic characteristics of a piezoelectric solar cell based on core-shell NW. (e) Schematic diagram of solar cell device based on piezoelectrically polarized core-shell NW arrays, which are synthesized on a conductive substrate. (a)–(e) Reproduced with permission [66]. Copyright 2010, ACS.

$\pi/2$  around the  $z$  axis. This demonstrates that the strain components  $\epsilon_{xx}$  and  $\epsilon_{yy}$  are constant and only distribute in the core area, whereas  $\epsilon_{zz}$  gradually becomes constant along the  $z$  axis. Figure 5(c) illustrates the effective piezoelectric charge density by numerically computed, which is non-sequence at the interface of core/shell materials due to the discontinuous relative permittivity of different materials. It can be clearly seen in figure 5(d) that the axial piezoelectric field induced by the inner strain of compound semiconductor core-shell nanowires can be employed for modulating photocurrent through the NW. In addition, the magnitude of the piezoelectric field depends on not only the core and shell materials but also the ratio of core and shell radius. Figure 5(e) shows the large-area solar cells based on arrays of piezoelectric core-shell NWs, in which the back contact is a heavily doped semiconductor substrate and the top contact is a transparent conducting film. When the device is under sunlight, photon-generated carriers (electrons and holes) will be separated by the piezoelectric fields generated in the core-shell NWs, and therefore a photocurrent will be created in the circuit. The proposed core-shell NWs here possess an inherent piezoelectric property, which could be employed efficiently for solar energy conversion. In

addition, the new design of core-shell NWs based solar cell has obvious advantages in device fabrication compared with previous photovoltaic devices based on NWs, for which a p-n junction is essential.

#### 4.2. Piezoelectric charge enhanced performance of graded InGaN nanowire solar cells

InGaN, with high carrier mobility, large saturation velocity, high absorption co-efficient ( $10^5\text{ cm}^{-1}$ ), and strong radiation resistance, has become a potential candidate for high performance solar cells owing to its wide direct bandgap (0.7–3.4 eV), which covers the major section of the solar spectrum. Since the synthesis of ideal p-InGaN for the application of solar cells is limited by several key factors, a p-GaN/n-In<sub>x</sub>Ga<sub>1-x</sub>N heterojunction has been proposed to replace the homojunction. However, the large amounts of piezoelectric charges ( $P_{pz}$ ) in the GaN/In<sub>x</sub>Ga<sub>1-x</sub>N heterojunction will generate a piezoelectric field, opposing the built-in electric field of the p-n junction and decreasing the carrier collection efficiency. Golam Sarwar *et al* have demonstrated that for a p-GaN/unintentionally doped (UID)-In<sub>0.3</sub>Ga<sub>0.7</sub>N NW

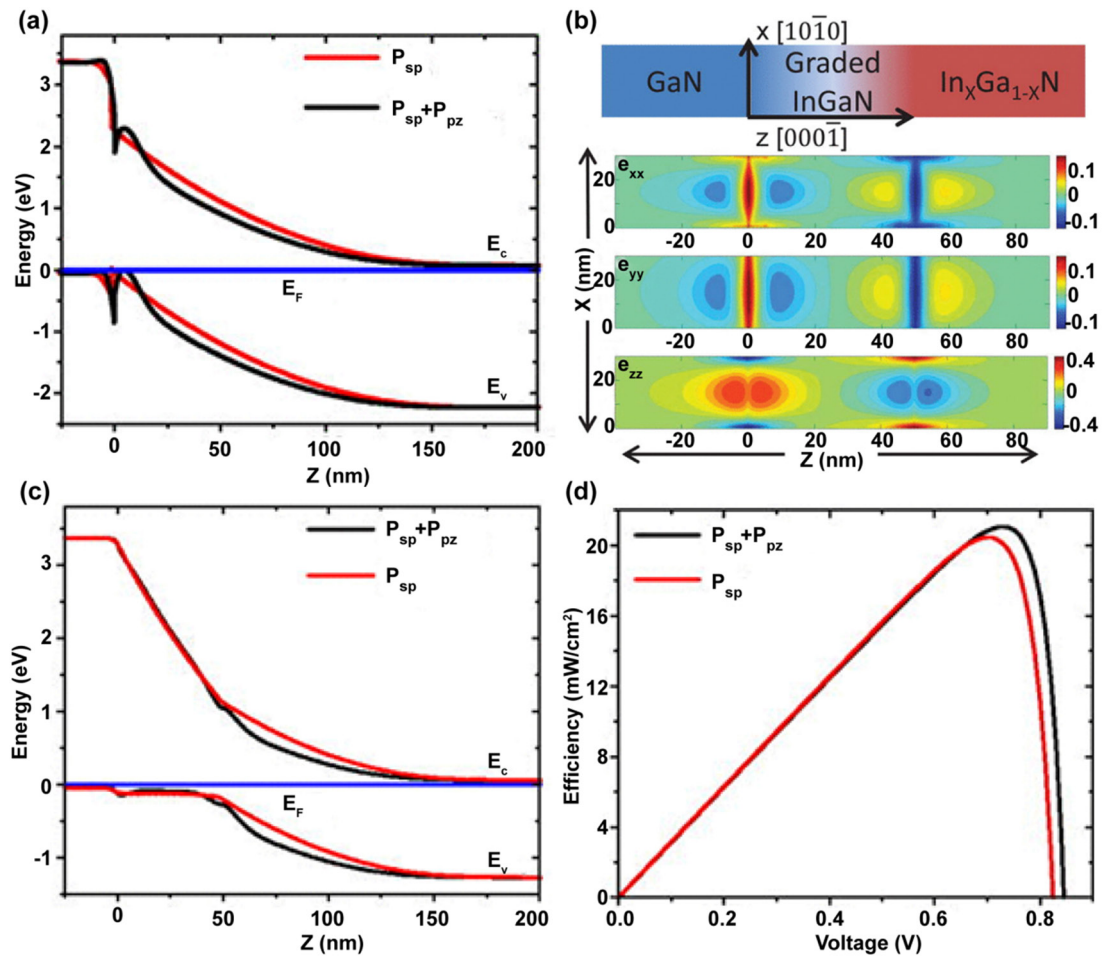


**Figure 6.** (a) Schematic illustration of equilibrium energy band diagram of p-GaN/UID-In<sub>0.3</sub>Ga<sub>0.7</sub>N NW solar cell. (b) Schematic diagram and distribution (in %) of strain components ( $e_{xx}$ ,  $e_{yy}$ , and  $e_{zz}$ ) of GaN/graded-InGaN/In<sub>x</sub>Ga<sub>1-x</sub>N NW solar cell. (c) Equilibrium energy band diagram of p-GaN/UID-graded-InGaN/UID-In<sub>0.65</sub>Ga<sub>0.35</sub>N NW solar cell. (d) Power density–voltage characteristic of a GaN/UID-graded-InGaN/UID-In<sub>0.65</sub>Ga<sub>0.35</sub>N NW solar cell. (a)–(d) Reproduced with permission [67]. Copyright 2012, AIP.

solar cell, the maximum numerical simulation of the strain components of  $e_{xx}$ ,  $e_{yy}$ , and  $e_{zz}$  are 1.69%, 1.69%, and 1.11%, respectively [67]. Figure 6(a) illustrates that the valence band at the p-GaN/n-In<sub>x</sub>Ga<sub>1-x</sub>N interface is discontinuous and the increased energy barrier impedes hole transport, resulting in a degraded performance of the solar cell. To avoid this deterioration, a graded layer was inserted between the p-GaN and n-In<sub>x</sub>Ga<sub>1-x</sub>N absorption layers, which can be seen in figure 6(b). The strain in the graded junction NW decreases compared to the abrupt junction NW due to the spontaneous polarization charge ( $P_{sp}$ ) being uniformly distributed in this graded junction. The maximum strain components of  $e_{xx}$ ,  $e_{yy}$ , and  $e_{zz}$  are 0.18%, 0.18%, and 0.48% respectively, which is  $\sim 6\times$  smaller than abrupt heterostructures. Meanwhile the valence band and conduction band from p-GaN to UID n-In<sub>0.65</sub>Ga<sub>0.35</sub>N became smooth, as shown in figure 6(c). In this structure, the UID InGaN graded layer becomes p-type under the effect of  $P_{sp}$ . Besides, the strain-induced piezoelectric charge  $P_{pz}$  can increase the hole concentration and the built-in-potential, accordingly enhancing the efficiency and power density of the graded NW solar cell, which can be seen from the black line present in figure 6(d). This work investigates the effect of piezoelectric charge on two different

solar cells and proposes a new method to increase the overall performance of the nanowire solar cells by exploiting piezoelectric charge in the p-type InGaN graded region.

#### 4.3. Enhanced Cu<sub>2</sub>S/CdS coaxial nanowire solar cells by piezo-phototronic effect

As reviewed previously, core–shell piezoelectric semiconductor NWs are promising candidates for solar cells modulated by the *piezo-phototronic effect* [68]. After the theoretical study on piezoelectric effect on core–shell NW photovoltaic (PV) devices by Xu’s group [65, 66], the first experimental verification using n-CdS/p-Cu<sub>2</sub>S coaxial NWs as PV devices had been carried out by Pan *et al* [69], in which our group successfully tuned the performance of the PV devices by *piezo-phototronic effect* and proposed a new concept for improving the conversion efficiency of solar cells. The fabrication process of the NW PV devices is shown in figure 7(a): a vapor–liquid–solid (VLS) synthesized n-CdS NW was partly cation replaced by dipping it into the CuCl solution with one end packaged by epoxy to obtain the n-CdS/p-Cu<sub>2</sub>S coaxial NWs. The PV device was manufactured on a polyethylene terephthalate (PET) substrate and showed an excellent flexibility.

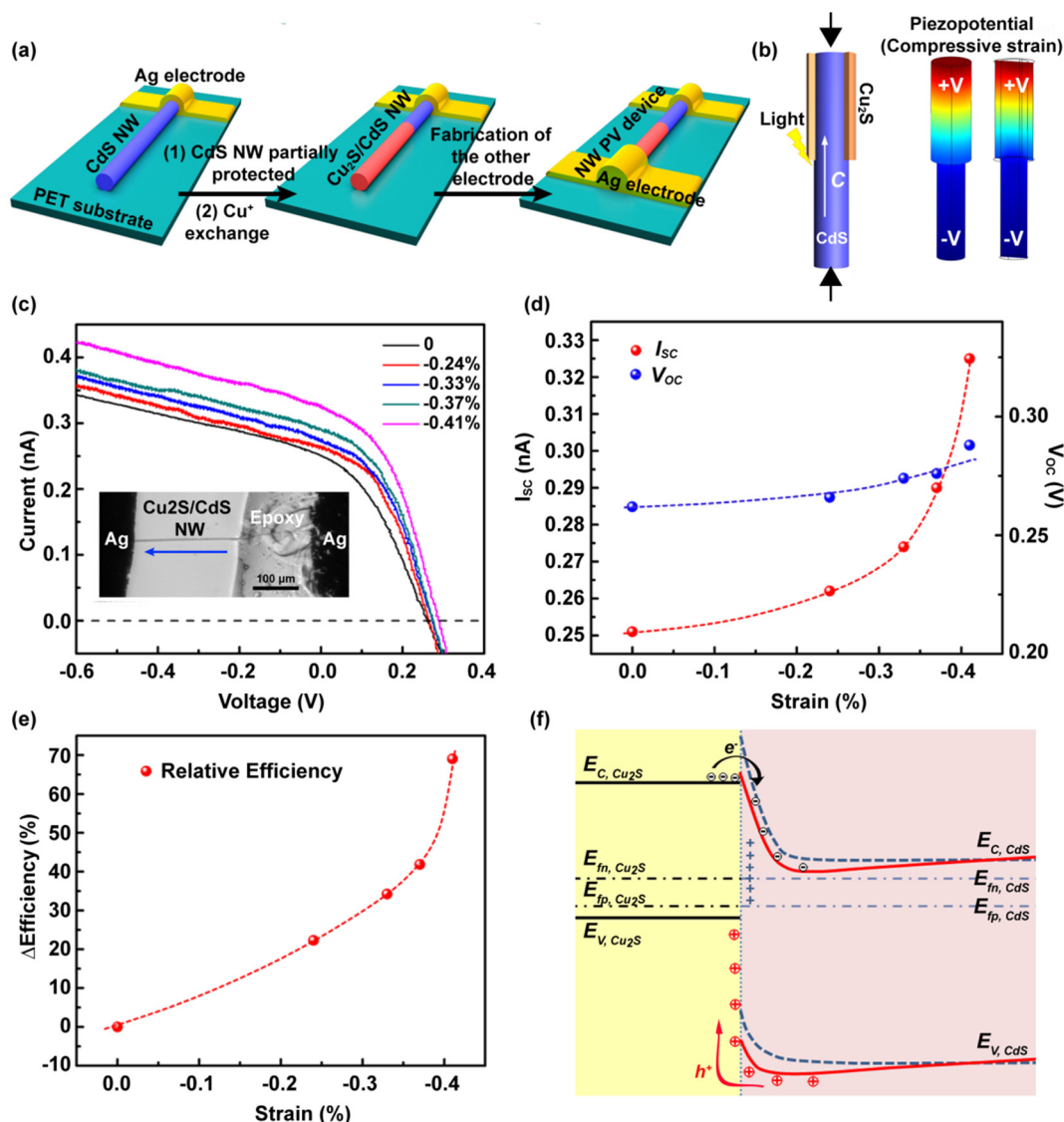


**Figure 7.** (a) Schematic diagram of the fabrication process of the CdS/Cu<sub>2</sub>S coaxial NW solar cell. From left to right, a CdS (blue) NW with metal electrode at one end is partially dipped into CuCl solution to form Cu<sub>2</sub>S (pink) shell, on which the other metal contact was fabricated. (b) Schematics and numerically calculated piezopotential distribution of a core–shell piezoelectric NW solar cell under compressive strain in configuration (I). (c) The *I*–*V* curve of the CdS/Cu<sub>2</sub>S coaxial NW solar cell under varying compressive strain, and the insert shows an optical microscopy image of the Cu<sub>2</sub>S/CdS coaxial NW solar cell. The open circuit voltage, the short circuit current (d), and relative efficiency (e) change with the applied strain. (f) The energy band diagram of a solar cell based on coaxial piezoelectric NW under compressive strain in configuration (I). (a)–(f) Reproduced with permission [69]. Copyright 2012, ACS.

Since the CdS NW is in asymmetric polarity [64], two different configurations are formed after the cation conversion: one is Cu<sub>2</sub>S shell only fabricated at the +*c* axis end of the CdS NW, named as configuration I; the other is Cu<sub>2</sub>S shell only fabricated at the –*c* axis end of the CdS NW, named as configuration II. Taking configuration I for example (figure 7(b)), when the applied compressive strain increases from zero to –0.41%, the current versus voltage curves change regularly, as shown in figure 7(c). The *I*<sub>sc</sub> increased from 0.25 to 0.33 nA, while the *V*<sub>oc</sub> changed between 0.26 and 0.29 V (figure 7(d)), thus resulting in 70% increase of the relative convention efficiency of this solar cell, which can be seen in figure 7(e). The schematic structure of configuration I and the corresponding energy band diagram of the piezoelectric

core–shell NW PV device upon compressive strain are shown in figure 7(f). It can be seen that the barrier height at the CdS/Cu<sub>2</sub>S heterojunction interface decreased obviously under external compressive strain, which might accelerate the separation of electron–hole pairs and reduce the possible recombination, and thus enhance the overall performance of the core–shell PV device. For configuration II, the performance of this PV device decreased with the increased external compressive strain. When applied compressive strain up to 0.5%, the *I*<sub>sc</sub> decreased from 3.47 to 3.05 nA and the *V*<sub>oc</sub> changed between 532 and 545 mV, thereby the energy conversion efficiency decreased by about 15%. This study suggests a new possibility—to modulate the performance of a core–shell NW solar cell through the *piezo-phototronic effect*.

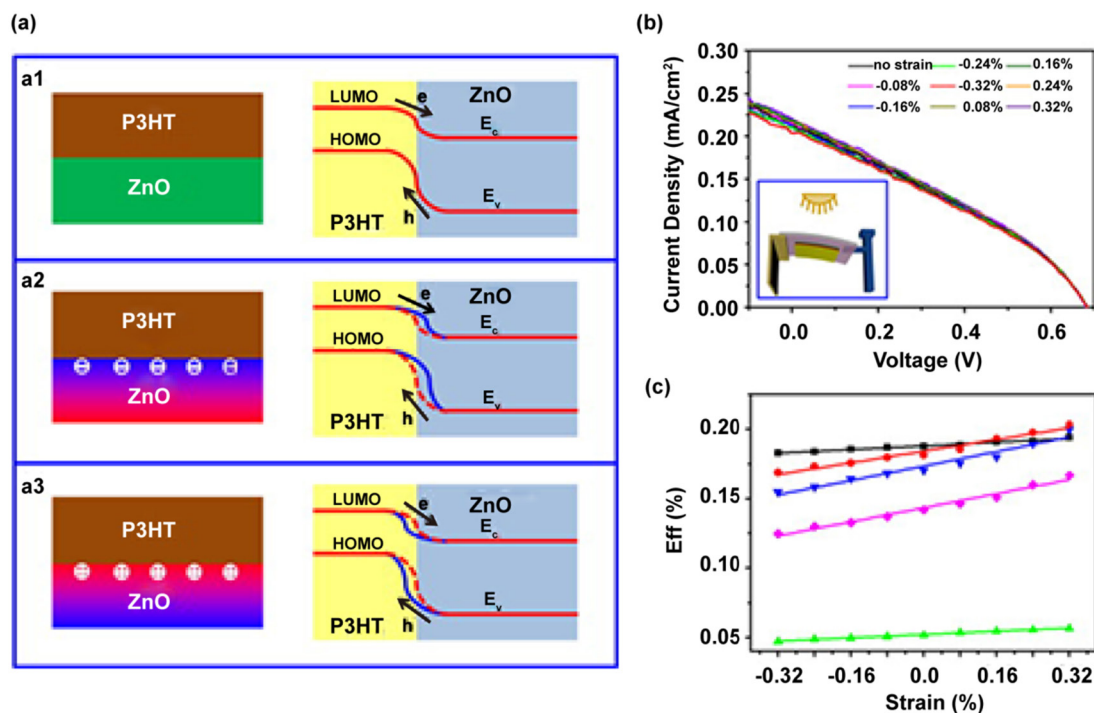


**Figure 8.** (a) Schematics and energy band diagram of the ZnO/P3HT solar cell in general condition (a1) and under different polarization strain ((a2) and (a3)). Blue and red lines represent the band structure with and without strain. (b) The performance of a solar cell under different applied strains, and the inset illustrates the measurement setup. (c) Strain-efficiency scatter diagram and linear fitting for each group. (a)–(c) Reproduced with permission [71]. Copyright 2013, Elsevier Ltd.

## 5. Piezo-phototronic effect enhanced performance of organic/inorganic solar cells

### 5.1. Effective piezo-phototronic enhancement of ZnO/P3HT solar cells

Organic/inorganic solar cells have become the focus of one of the most interesting and potential research fields due to their special properties, combining organics with semiconductors [70]. The *piezo-phototronic effect* in ZnO/P3HT solar cell systems has been researched; furthermore, the detailed influence of crystallization and doping level of ZnO on the *piezo-phototronic effect* as well as the performance of solar cell has been discussed by Wen *et al* [71]. n-ZnO film was deposited by RF sputtering and then P3HT was spin coated onto the ZnO layer as the p-type material, the band structure of the ZnO/P3HT interface is described in figure 8(a1). Under external strain, both the conduction and valence bands of ZnO in the junction region are raised due to the induced negative polarization charges as shown in figure 8(a2), consequently reducing the built-in electric field and suppressing the separation of photon-generated carriers, resulting in a decrease of  $J_{sc}$ , as labelled in figure 8(b). In contrast, strain induced positive polarization charges will lower the conduction and valence bands in the junction region (figure 8(a3)) and thus lead to a higher built-in electric field and an increase of  $J_{sc}$  (figure 8(b)). Meanwhile the open-circuit voltage ( $V_{oc}$ ) stays almost constant under different strains, because  $V_{oc}$  is mainly determined by the difference between quasi-Fermi levels of the p-type and n-type materials, which is strongly affected by the illumination intensity.

To further improve the *piezo-phototronic effect* in the ZnO/P3HT solar cells, five different groups of samples were studied, with different crystallization and doping levels of ZnO. Detailed research has been carried out on the variation of the short-circuit current density ( $J_{sc}$ ), open-circuit voltage ( $V_{oc}$ ), efficiency (figure 8(c)) and fill factor with the different applied strain; the results clearly show that the optimized performance can be achieved under the tensile strain of 0.32%, with the ZnO film sputtered at 120 W, 6 mTorr, 30 sccm Ar, 10 sccm O<sub>2</sub> and the substrate heated to 120 °C. Overall, the principle and regularities provided in this study could be applicable to solar cell systems including piezoelectric semiconductor materials, which is meaningful in further enhancing performances of the solar cell devices by introducing external strain.

### 5.2. Piezo-phototronic effect on ZnO/PEDOT:PSS hybrid structure

Another organic/inorganic structure based on a ZnO micro/nanowire and poly (3,4-ethylenedioxythiophene)/polystyrene sulfonate (PEDOT:PSS) on a flexible polystyrene (PS) substrate has been studied as the solar cell devices modulated by *piezo-phototronic effect* by Zhang *et al* [72]. Figure 9(a) illustrates the schematic diagram of the hybrid structure solar cell and the testing equipment, a single ZnO micro/nanowire was first placed on a PS substrate, then with one end covered with PEDOT:PSS film and the other end fixed with silver paste [72]. Figure 9(b) represents the measured current under periodical solar light exposure and it suggests that this hybrid structure device has a good response to solar illumination.

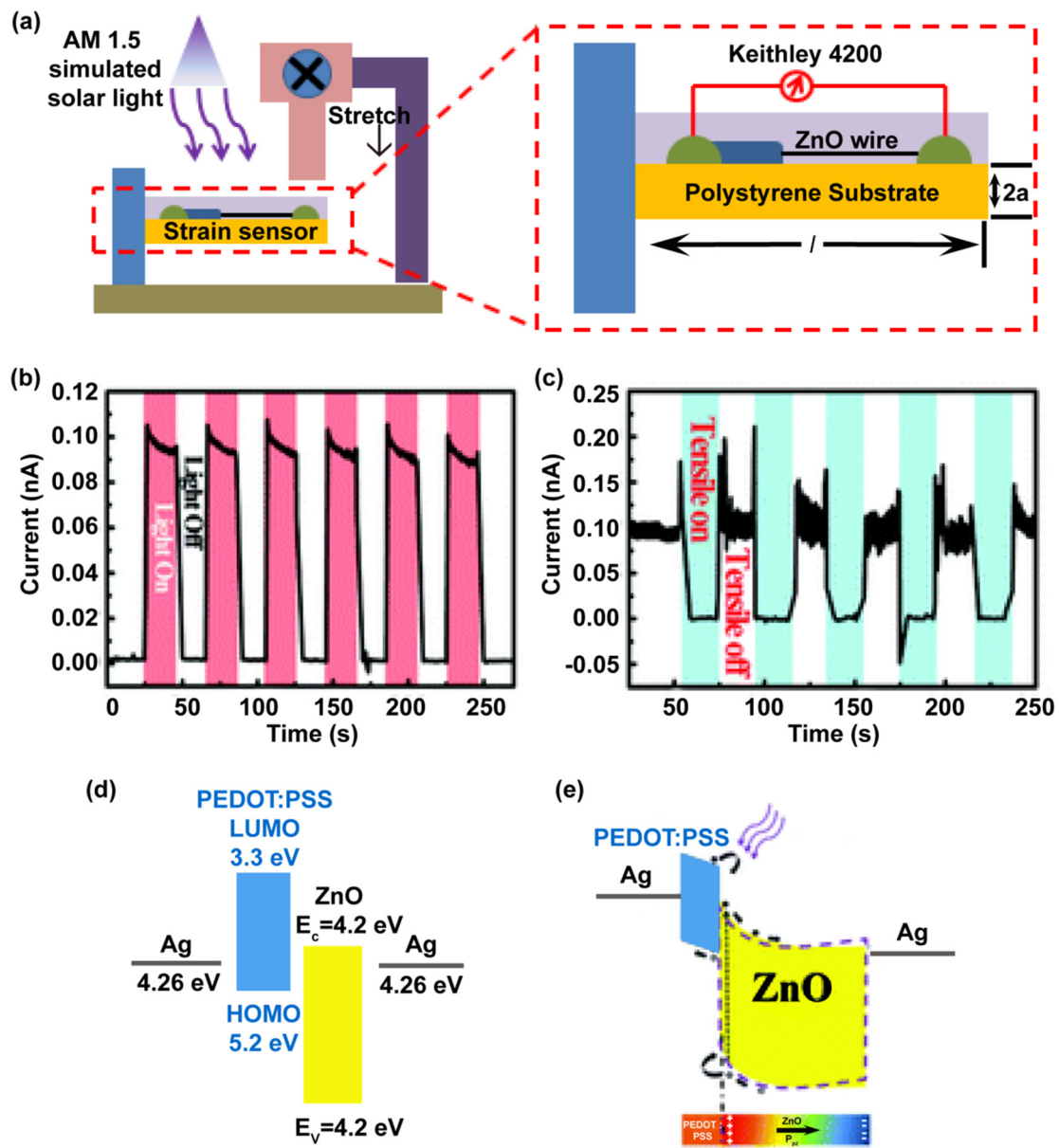


**Figure 9.** (a) Schematic diagram of the measurement system for the electromechanical characteristics of the device. (b) Photocurrent variation under periodic irradiation of sunlight on the device. (c) Current response of the device to regular tensile strains, with solar light illumination. (d) Original energy band diagrams of Ag, PEDOT:PSS and ZnO in this device. (e) Modified energy band diagram of ZnO upon tensile strain and illumination of solar light simultaneously. (a)–(e) Reproduced with permission [72]. Copyright 2013, RSC.

When an external stretched strain was applied to the device under AM 1.5 illumination of solar light simulator, the corresponding current as a function of time is shown in figure 9(c), which indicates that the response time and reset time of the solar cell are 3.7 s and 3.8 s respectively, resulting in a sensitivity as high as  $1.0 \times 10^4$ . The strain induced current change is mainly due to the *piezo-phototronic effect* of ZnO as well as the band structure change, which is illustrated in figures 9(d) and (e) in detail. The original energy band structure of Ag electrode, PEDOT:PSS layer and ZnO micro/nanowire is shown in figure 9(d). Under solar illumination and upon stretch strain, the induced positive piezoelectric polarization charges in ZnO side will lower the conduction band of ZnO at the interface region (figure 9(e)) and thus lead to a lower

current. Conversely, while applying compressive strain, negative piezoelectric charges will generate in the interface, which results in a higher current accordingly.

### 5.3. Piezo-phototronic effect on polymer/ZnO nanorod photovoltaic device

Dunn *et al* investigated the influence of acoustic vibration on the performance of photovoltaic devices based on the polymer/ZnO nanorod system [73]. They prepared five types of ZnO nanorods with different aspect ratios and fabricated P3HT/ZnO nanorod heterojunction solar cells correspondingly. The efficiency measurement results of these devices are shown in figure 10(a), and they found that with the increase of aspect

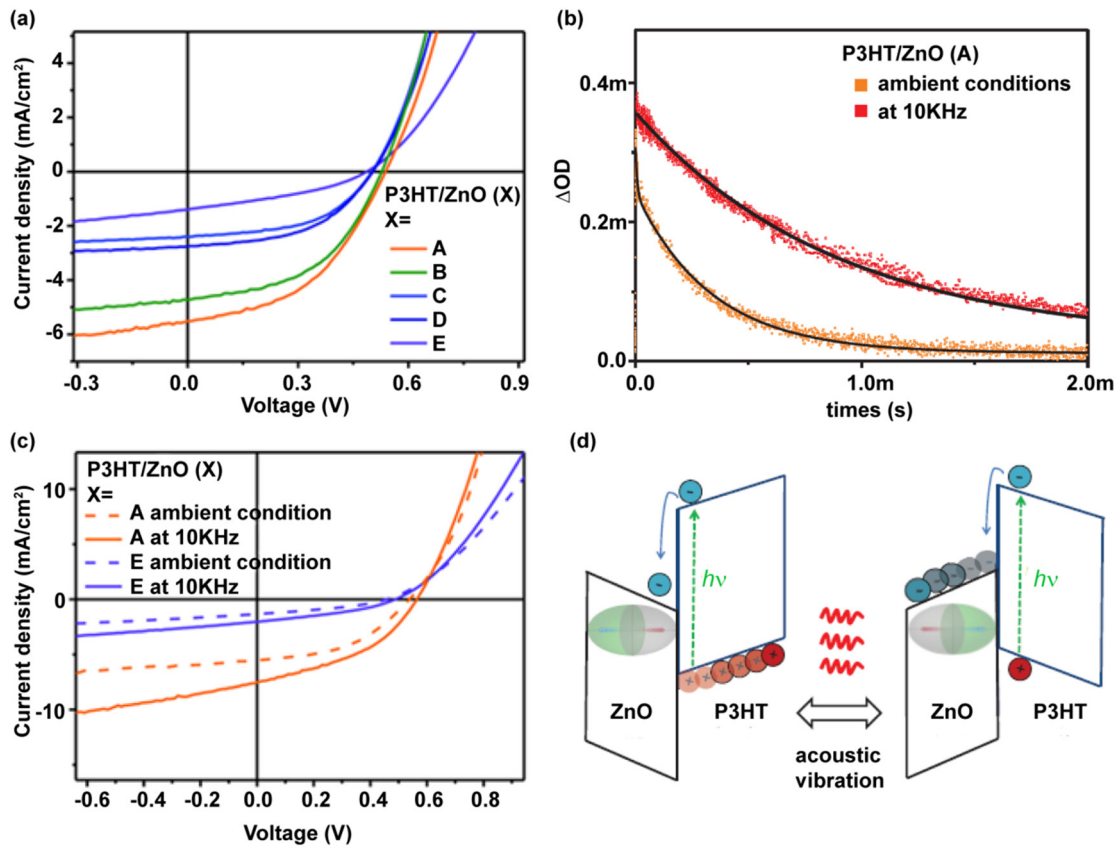


**Figure 10.** (a)  $J$ - $V$  characteristics of P3HT/ZnO (X) with different aspect ratios, A: 38, B: 30, C: 20, D: 19, E: 5. (b) Transient absorption signals of P3HT/ZnO (A) with and without external frequency of 10kHz at 75 dB, where the changed y-axis represents a change in the yield of photon-generated charges. (c)  $J$ - $V$  characteristics of P3HT/ZnO (A) and P3HT/ZnO (E) devices with and without external frequency of 10 KHz. (d) Schematic band diagram of P3HT/ZnO nanorod system, indicating the impact of piezopotential induced by oscillating acoustic vibration. (a)–(d) Reproduced with permission [73]. Copyright 2013, WILEY-VCH.

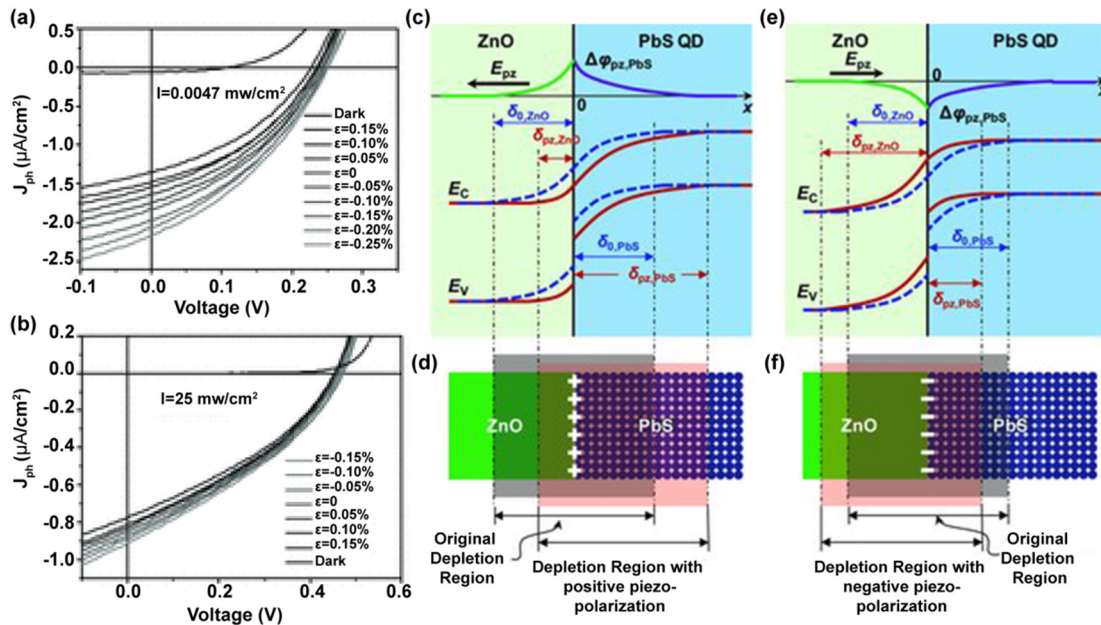


**Figure 11.** (a)  $J$ - $V$  curves of a ZnO/PbS QDSC under different compressive and tensile strains, with  $0.0047 \text{ mW cm}^{-2}$  illumination. (b)  $J$ - $V$  curves of a ZnO/PbS QDSC under different compressive and tensile strains, with  $25 \text{ mW cm}^{-2}$  illumination. Band diagram of the QDSC with the positive  $P_{pz}$  (c) and negative  $P_{pz}$  (e) at the ZnO/PbS interface,  $\delta_0$  and  $\delta_{pz}$  represent the width of the depletion regions without and with the piezopotential respectively. (d) and (f) Schematic diagram of the depletion regions changes in ZnO/PbS-QD accordingly. (a)–(d) Reproduced with permission [74]. Copyright 2013 WILEY-VCH.

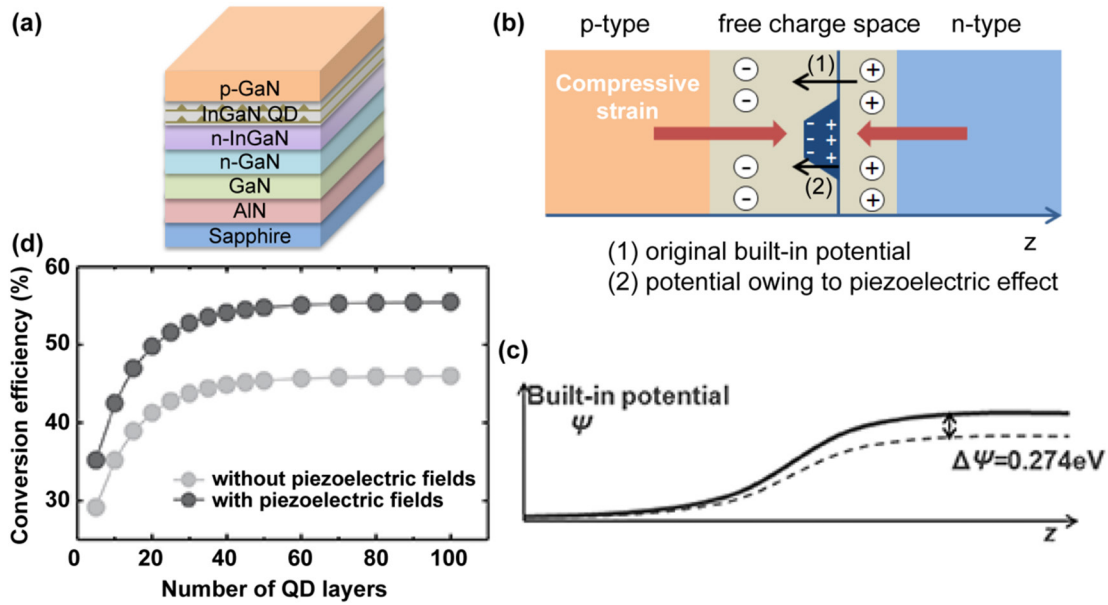


**Figure 12.** (a) Schematic diagrams of the structure of QD-IBSC, with InGaN QD. The electric fields (b) and the built-in potential (c) in the p–n junction based solar cell. In (c) the solid line and the dashed line represent the built-in potential with and without the piezoelectric fields. (d) Compared conversion efficiency of the InGaN based QD-IBSCs with and without the piezoelectric fields. (a)–(d) Reproduced with permission [75]. Copyright 2015, IOP.

ratio, the short-circuit current density increased significantly, which might benefit from the increased interface area of ZnO/P3HT.

Then they utilized the optimal aspect ratio and further applied acoustic vibration to samples A and E to investigate possible variations in the mechanical response. They observed an obvious enhanced performance and a longer decay lifetime (from 0.34 ms to 0.88 ms) in the device when under external vibration (~10 kHz), which can be seen in figures 10(b) and (c) respectively, and analogous properties were also found in other polymer/ZnO systems, while no dependence on the external vibration was seen in the P3HT/PCBM system, which means the enhancement observed under acoustic stress is owing to the charge separation in the polymer/ZnO heterojunction interface.

They also illustrated the suggested mechanism in these phenomena, as shown in figure 10(d). When the ZnO nanorods are under external vibration, polarization fields will occur across these nanorods, the electric fields will drive the electrons in ZnO or holes in P3HT away from their interface, thus reducing the charge carrier recombination losses and eventually enhancing the overall performance of the device. This work gives an expansion on various photovoltaic devices that employ high aspect ratio nanostructures with piezoelectric effect.

## 6. Piezo-phototronic effect enhanced performance of quantum-dot solar cells

### 6.1. Enhanced photovoltaic performance in depleted-heterojunction quantum-dot solar cells

Shi *et al* studied piezoelectric-polarization ( $P_{pz}$ ) modulated depletion-heterojunction quantum dot solar cells (DH QDSCs) based on the ZnO/PbS system [74]. They obtained enhanced performance in n-ZnO/p-PbS based quantum dot

photovoltaic devices by introducing  $P_{pz}$  at the heterojunction interface. Figures 11(a) and (b) show the  $J$ – $V$  characteristics of the QDSC under different external strains. Under the illumination intensity of  $0.0047 \text{ mW cm}^{-2}$  using a solar simulator, they obtained an efficiency of  $\approx 4.0\%$  at a  $-0.25\%$  compressive strain, while the efficiency is  $\approx 3.1\%$  under zero strain, which means the improvement of the efficiency can be as high as 30%. Besides, the efficiency also exhibited a linear response to the strain applied to the device, and with each 0.01% strain drop, the efficiency got a 1.2% enhancement. They further tested the devices under a higher illumination flux ( $25 \text{ mW cm}^{-2}$ ); however, they only obtained a 0.55% efficiency enhancement per 0.01% strain drop. The efficiency decrease phenomenon at the higher illumination intensity is consistent with the light-intensity-dependent photovoltaic performance in other solar cell systems.

It can be clearly seen from the results that the efficiency of the QDSC in both illumination cases could be enhanced by compressive strain. The working principle behind these phenomena could be seen by the band diagrams in figure 11. Figures 11(c) and (d) represent the case where the positive  $P_{pz}$  are generated at the ZnO/PbS interface, and the positive  $P_{pz}$  can effectively enlarge the depletion zone on the PbS QD side, and result in a narrower depletion region and shallower band deformation in the ZnO layer, eventually enhancing charge extraction at the ZnO/PbS interface, and regulating the overall performance of the QDSC. Conversely, in the negative  $P_{pz}$  case, which can be seen in figures 11(e) and (f), the generated negative  $P_{pz}$  will shrink the depletion region in PbS, jeopardize the charge extraction and decrease the PV efficiency in the end. The *piezo-phototronic effect* modulation strategy put forward in this work gives a new insight into improvement of the carrier transportation properties of heterojunction based devices by introducing  $P_{pz}$ .

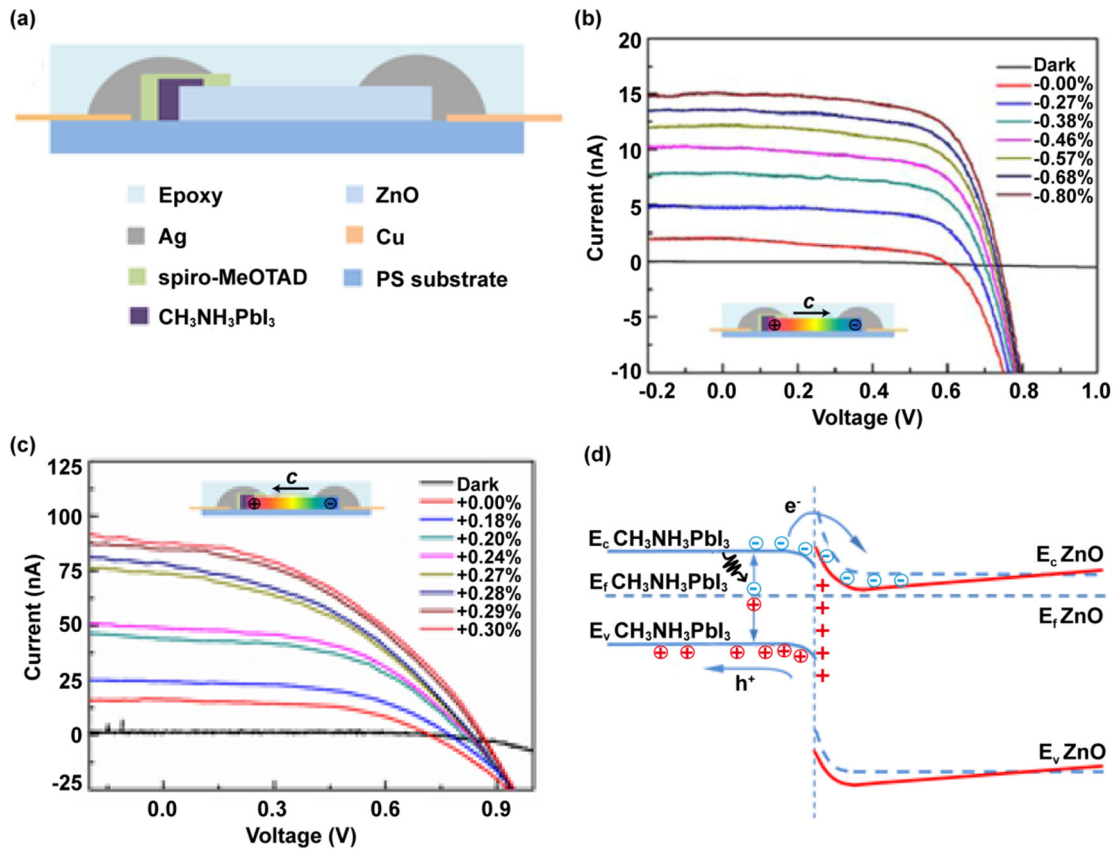


**Figure 13.** (a) Structure diagram of the ZnO NW/perovskite solar cell. (b)  $I$ - $V$  characteristics of the ZPSC-I under different compressive strain. (c)  $I$ - $V$  characteristics of the ZPSC-II under different stretch strain. (d) The corresponding energy band diagram with the piezopotential distributions in the compressed device of ZPSC-I and in stretched device of ZPSC-II. (a)–(d) Reproduced with permission [78]. Copyright 2016, Elsevier Ltd.

6.2. Piezoelectric field enhanced InGaN based intermediate band solar cells

Tang *et al* studied the influence of piezoelectric field on InGaN quantum dot based intermediate band solar cells (IBSCs) [75]. They designed a QD-IBSC structure based on InGaN, as shown in figure 12(a), where the n-GaN layer is fabricated on a standard undoped GaN buffer, and an  $In_{0.4}Ga_{0.6}N$  layer is used as a strain-balanced layer, then the multiple QD layers with  $In_{0.4}Ga_{0.6}N$ :barrier/ $In_{0.8}Ga_{0.2}N$ :QDs is followed, and finally a p-GaN is capped on the top of the structure. All these processes can be conducted through metal-organic chemical vapor deposition (MOCVD).

On the basis of this structure, they calculated the piezoelectric fields in the InGaN/GaN system. Figure 12(b) illustrated the electric fields in the p-n junction, where a compressive strain is applied on the p-GaN, it will produce a piezoelectric field along the same direction as the built-in electric fields, which leads to an increase of the built-in potential, which is also shown in figure 12(c). When the number of the designed InGaN QD structure is ten-period, the open circuit voltage of the solar cell device could be enhanced by 0.274V and the conversion efficiency is improved by 20%, from 35.2% to 42.5%, because of the piezoelectric fields, which can be seen in figure 12(d). Apart from this, the conversion efficiency of the IBSC is calculated to saturate at 46.0% without piezoelectric fields, while this value could increase

to 55.4% due to the piezoelectric fields. The results presented in this work give a clear understanding on the piezoelectric effect, and pave the way for developing new methods to push the efficiency limit and enhance the overall performance of InGaN based thin film solar cells.

7. Piezo-phototronic effect enhanced perovskite solar cells

Perovskite solar cells are recognized as one of the most promising photovoltaic devices in recent years, researchers have found numerous ways to improve their overall performances [76, 77]. Among them, Guofeng Hu and Caofeng Pan *et al* put forward a new but effective method, that the performance of the ZnO microwire based flexible perovskite solar cells could be enhanced by the *piezo-phototronic effect* [78]. Our group used single ZnO microwire as electron transport material, where the piezoelectric ZnO microwire can form a heterojunction with the perovskite material; the corresponding schematic of a fabricated device is illustrated in figure 13(a). Our group studied the performance of the single ZnO microwire based perovskite solar cells under different constant and variable external strains. It can be concluded that the power conversion efficiency of the perovskite solar cells with the *c*-axis of ZnO pointing away from perovskite (ZPSC-I), can be enhanced by 1280% (from 0.0216% to

0.298%) under compressive strain as shown in figure 13(b); while the efficiency of the devices with the *c*-axis of ZnO pointing towards the perovskite (ZPSC-II) can be enhanced by 417.650% (from 0.068% to 0.3%) under tensile strain as shown in figure 13(c). Their corresponding band diagram can be seen in figure 13(d), the theory analysis shows that when the ZnO microwire is under strain, the local energy band of ZnO will be lowered by piezoelectric effect, which leads to a decreased barrier height at the ZnO/perovskite interface. This change will accelerate the separation of the photon-generated electron-hole pairs and decrease the possibility of recombination, eventually enhancing the overall performance of the solar cell.

## 8. Conclusion and outlook

In this paper, we have introduced the basic concept of the *piezo-phototronic effect*, and reviewed recent research progress in *piezo-phototronic effect* enhanced photovoltaic materials or solar cell devices. For devices using piezoelectric semiconductor materials, their current density could be significantly modulated by the *piezo-phototronic effect* under proper external strain, due to the changed energy level in the local interface region, and on this basis enhanced performance of solar cells can be achieved.

The description of the *piezo-phototronic effect* provided in this review gives a new perspective on improving the overall properties of solar cells that employ piezoelectric semiconductor materials by introducing external strain, which is of great significance in widespread applications, such as wearable technology, portable electronics, integrated optoelectronics, and defense technology.

## Acknowledgments

We thank Professor Zhonglin Wang (Beijing Institute of Nanoenergy and Nanosystems, Georgia Institute of Technology) for technical assistance and invaluable advice in our experiments and paper writings.

The authors are thankful for support from the ‘Thousand Talents’ program of China for pioneering researchers and innovative teams and from the President Funding of the Chinese Academy of Sciences, National Natural Science Foundation of China (No. 51432005, 61405040, 61505010 and 51502018), Beijing City Committee of science and technology (Z151100003315010), Beijing Natural Science Foundation (2164077 and 2164076).

## References

- [1] Akyildiz I F, Su W, Sankarasubramanian Y and Cayirci E 2002 Cayirci: ‘wireless sensor networks: a survey *Int. Symp. Comput. Netw.* **38** 393–422
- [2] Kou L, Huang T, Zheng B, Han Y, Zhao X, Gopalsamy K, Sun H and Gao C 2014 Coaxial wet-spun yarn supercapacitors for high-energy density and safe wearable electronics *Nat. Commun.* **5** 3754
- [3] Pan C, Li Z, Guo W, Zhu J and Wang Z L 2011 Fiber-based hybrid nanogenerators for/as self-powered systems in biological liquid *Angew. Chem. Int. Ed.* **50** 11192–6
- [4] Wang Z L, Zhu G, Yang Y, Wang S and Pan C 2012 Progress in nanogenerators for portable electronics *Mater. Today* **15** 532–43
- [5] Son D *et al* 2014 Multifunctional wearable devices for diagnosis and therapy of movement disorders *Nat. Nanotechnol.* **9** 397–404
- [6] Nour E S, Sandberg M O, Willander M and Nur O 2014 Handwriting enabled harvested piezoelectric power using ZnO nanowires/polymer composite on paper substrate *Nano Energy* **9** 221–8
- [7] Wang X, Dong L, Zhang H, Yu R, Pan C and Wang Z L 2015 Recent progress in electronic skin *Adv. Sci.* **2** 1500169
- [8] Lee Y-H *et al* 2013 Wearable textile battery rechargeable by solar energy *Nano Lett.* **13** 5753–61
- [9] Que M 2014 Flexible quantum dot-sensitized solar cells employing CoS nanorod arrays/graphite paper as effective counter electrodes *J. Mater. Chem. A* **2** 13661–6
- [10] Pan C, Luo J and Zhu J 2011 From proton conductive nanowires to nanofuel cells: a powerful candidate for generating electricity for self-powered nanosystems *Nano Res.* **4** 1099–109
- [11] Guo W, Xu C, Zhu G, Pan C, Lin C and Wang Z L 2012 Optical-fiber/TiO<sub>2</sub>-nanowire-arrays hybrid structures with tubular counterelectrode for dye-sensitized solar cell *Nano Energy* **1** 176–82
- [12] Zhou Y 2012 Enhancement of photovoltaic effect in nanoscale polarization graded ferroelectrics *Sol. Energy* **86** 811–5
- [13] Brendel R and Queisser H J 1993 On the thickness dependence of open circuit voltages of p–n junction solar cells *Sol. Energy Mater. Sol. Cells* **29** 397–401
- [14] Zhang F, Liu X, Pan C and Zhu J 2007 Nano-porous anodic aluminium oxide membranes with 6–19 nm pore diameters formed by a low-potential anodizing process *Nanotechnology* **18** 12872
- [15] Godfrey R B and Green M A 1979 655 mV open-circuit voltage, 17.6% efficient silicon MIS solar cells *Appl. Phys. Lett.* **34** 790
- [16] Pan C *et al* 2011 Wafer-scale high-throughput ordered arrays of Si and coaxial Si/Si<sub>1-x</sub>Ge<sub>x</sub> wires: fabrication, characterization, and photovoltaic application *ACS Nano* **5** 6629–36
- [17] Chen H-Y, Hou J, Zhang S, Liang Y, Yang G, Yang Y, Yu L, Wu Y and Li G 2009 Polymer solar cells with enhanced open-circuit voltage and efficiency *Nat. Photon.* **3** 649–53
- [18] Lee M M, Teuscher J, Miyasaka T, Murakami T N and Snaith H J 2012 Efficient hybrid solar cells based on meso-structured organometal halide perovskites *Science* **338** 643
- [19] Yang W S, Noh J H, Jeon N J, Kim Y C, Ryu S, Seo J and Seok S I 2015 SOLAR CELLS. High-performance photovoltaic perovskite layers fabricated through intramolecular exchange *Science* **348** 1234–7
- [20] Liu M, Johnston M B and Snaith H J 2013 Efficient planar heterojunction perovskite solar cells by vapour deposition *Nature* **501** 395–8
- [21] Pan C *et al* 2008 Nanowire-based high performance ‘micro fuel cell’: one nanowire, one fuel cell *Adv. Mater.* **20** 1644
- [22] Pan C *et al* 2010 Generating electricity from biofluid with a nanowire-based biofuel cell for self-powered nanodevices *Adv. Mater.* **22** 5388
- [23] Wang Z L and Wu W 2013 Piezotronics and piezo-phototronics: fundamentals and applications *Natl Sci. Rev.* **1** 62–90
- [24] Wang Z L, Yang R, Zhou J, Qin Y, Xu C, Hu Y and Xu S 2010 Lateral nanowire/nanobelt based nanogenerators, piezotronics and piezo-phototronics *Mater. Sci. Eng. R* **70** 320–9

- [25] Wang Z L 2012 From nanogenerators to piezotronics-A decade-long study of ZnO nanostructures *MRS Bull.* **37** 814–27
- [26] Yang Q, Wang W, Xu S and Wang Z L 2011 Enhancing light emission of ZnO microwire-based diodes by piezophototronic effect *Nano Lett.* **11** 4012–7
- [27] Pan C, Dong L, Zhu G, Niu S, Yu R, Yang Q, Liu Y and Wang Z L 2013 High-resolution electroluminescent imaging of pressure distribution using a piezoelectric nanowire LED array *Nat. Photon.* **7** 752–8
- [28] Yang Q, Liu Y, Pan C, Chen J, Wen X and Wang Z L 2013 Largely enhanced efficiency in ZnO nanowire/p-polymer Hybridized inorganic/organic ultraviolet light-emitting diode by piezo-phototronic effect *Nano Lett.* **13** 607–13
- [29] Yang Q, Guo X, Wang W, Zhang Y, Xu S, Lien D H and Wang Z L 2010 Enhancing sensitivity of a single ZnO micro-/nanowire photodetector by piezo-phototronic effect *ACS Nano* **4** 6285–91
- [30] Liu Y, Yang Q, Zhang Y, Yang Z and Wang Z L 2012 Nanowire piezo-phototronic photodetector: theory and experimental design *Adv. Mater.* **24** 1410–7
- [31] Hu Y, Zhang Y, Chang Y, Snyder R L and Wang Z L 2010 Optimizing the power output of a ZnO photocell by piezopotential *ACS Nano* **4** 4220–4
- [32] Shvydka D, Drayton J, Compaan A D and Karpov V G 2005 Piezo-effect and physics of CdS-based thin-film photovoltaics *Appl. Phys. Lett.* **87** 123505
- [33] Xu C, Pan C, Liu Y and Wang Z L 2012 Hybrid cells for simultaneously harvesting multi-type energies for self-powered micro/nanosystems *Nano Energy* **1** 259–72
- [34] Wang Z L and Song J H 2006 Piezoelectric nanogenerators based on zinc oxide nanowire arrays *Science* **312** 242–6
- [35] Wang Z L 2010 Piezopotential gated nanowire devices: piezotronics and piezo-phototronics *Nano Today* **5** 540–52
- [36] Dong L, Niu S, Pan C, Yu R, Zhang Y and Wang Z L 2012 Piezo-phototronic effect of cdse nanowires *Adv. Mater.* **24** 5470–5
- [37] Janotti A and Van de Walle C G 2009 Fundamentals of zinc oxide as a semiconductor *Rep. Prog. Phys.* **72** 126501
- [38] Wang Z L 2012 Progress in piezotronics and piezo-phototronics *Adv. Mater.* **24** 4632–46
- [39] Gao Z, Zhou J, Gu Y, Fei P, Hao Y, Bao G and Wang Z L 2009 Effects of piezoelectric potential on the transport characteristics of metal-ZnO nanowire-metal field effect transistor *J. Appl. Phys.* **105** 113707
- [40] Wang Z L 2012 *Piezotronics and Piezo-Phototronics* 24 (Berlin: Springer)
- [41] Brillson L J and Lu Y 2011 ZnO Schottky barriers and Ohmic contacts *J. Appl. Phys.* **109** 121301
- [42] Tung R T 2001 Recent advances in Schottky barrier concepts *Mater. Sci. Eng. R* **35** 1–138
- [43] Crowell C R and Sze S M 1966 Current transport in metal-semiconductor barriers *Solid-State Electron.* **9** 1035–48
- [44] Hu G, Zhou R, Yu R, Dong L, Pan C and Wang Z L 2014 Piezotronic effect enhanced Schottky-contact ZnO micro/nanowire humidity sensors *Nano Res.* **7** 1083–91
- [45] Pan C, Yu R, Niu S, Zhu G and Wang Z L 2013 Piezotronic effect on the sensitivity and signal level of Schottky contacted proactive micro/nanowire nanosensors *ACS Nano* **7** 1803–10
- [46] Gao Z, Zhou J, Gu Y, Fei P, Hao Y, Bao G and Wang Z L 2009 Effects of piezoelectric potential on the transport characteristics of metal-ZnO nanowire-metal field effect transistor *J. Appl. Phys.* **105** 113707
- [47] Weerasinghe H C, Huang F and Cheng Y-B 2013 Fabrication of flexible dye sensitized solar cells on plastic substrates *Nano Energy* **2** 174–89
- [48] Yang Q, Wu Y, Liu Y, Pan C and Wang Z L 2014 Features of the piezo-phototronic effect on optoelectronic devices based on wurtzite semiconductor nanowires *PCCP* **16** 2790–800
- [49] Yu R, Pan C, Hu Y, Li L, Liu H, Liu W, Chua S, Chi D and Wang Z L 2013 Enhanced performance of GaN nanobelt-based photodetectors by means of piezotronic effects *Nano Res.* **6** 758–66
- [50] Wang Z L 2008 Towards self-powered nanosystems: from nanogenerators to nanopiezotronics *Adv. Funct. Mater.* **18** 3553–67
- [51] Muller R S and Kamins T I 1977 Device electronics for integrated circuits *Device Electron. Integr. Circuits*
- [52] Zhang Y, Liu Y and Wang Z L 2011 Fundamental theory of piezotronics *Adv. Mater.* **23** 3004–13
- [53] Zhou R, Hu G, Yu R, Pan C and Wang Z L 2015 Piezotronic effect enhanced detection of flammable/toxic gases by ZnO micro/nanowire sensors *Nano Energy* **12** 588–96
- [54] Kim D Y, Lee S, Lin Z-H, Choi K H, Doo S G, Chang H, Leem J-Y, Wang Z L and Kim S-O 2014 High temperature processed ZnO nanorods using flexible and transparent mica substrates for dye-sensitized solar cells and piezoelectric nanogenerators *Nano Energy* **9** 101–11
- [55] Yu R, Dong L, Pan C, Niu S, Liu H, Liu W, Chua S, Chi D and Wang Z L 2012 Piezotronic effect on the transport properties of GaN nanobelts for active flexible electronics *Adv. Mater.* **24** 3532–7
- [56] Yu R, Wu W, Pan C, Wang Z, Ding Y and Wang Z L 2015 Piezo-phototronic Boolean Logic and computation using photon and strain dual-gated nanowire transistors *Adv. Mater.* **27** 940–7
- [57] Yu R, Pan C, Chen J, Zhu G and Wang Z L 2013 Enhanced performance of a ZnO nanowire-based self-powered glucose sensor by piezotronic effect *Adv. Funct. Mater.* **23** 5868–74
- [58] Chen C Q, Shi Y, Zhang Y S, Zhu J and Yan Y J 2006 Size dependence of Young's modulus in ZnO nanowires *Phys. Rev. Lett.* **96** 075505
- [59] Yu R, Wang X, Wu W, Pan C, Bando Y, Fukata N, Hu Y, Peng W, Ding Y and Wang Z L 2015 Temperature dependence of the piezophototronic effect in CdS nanowires *Adv. Funct. Mater.* **25** 5277–84
- [60] Hu Y, Klein B D, Su Y, Niu S, Liu Y and Wang Z L 2013 Temperature dependence of the piezotronic effect in ZnO nanowires *Nano Lett.* **13** 5026–32
- [61] Oregan B and Gratzel M 1991 A low-cost, high-efficiency solar-cell based on dye-sensitized colloidal TiO<sub>2</sub> films *Nature* **353** 737–40
- [62] Zhang Y, Yang Y and Wang Z L 2012 Piezo-phototronics effect on nano/microwire solar cells *Energy Environ. Sci.* **5** 6850
- [63] Sze S M 1981 *Physics of Semiconductor Devices* 51 (New York: Wiley)
- [64] Espinosa H D, Bernal R A and Minary-Jolandan M 2012 A review of mechanical and electromechanical properties of piezoelectric nanowires *Adv. Mater.* **24** 4656–75
- [65] Boxberg F, Søndergard N, Xu H Q, Wallentin J, Jin A, Trygg E, Borgström M, Ihm J and Cheong H 2011 Photovoltaics with piezoelectric core-shell nanowires *AIP Conf. Proc.* **1399** 469–70
- [66] Boxberg F, Søndergard N and Xu H Q 2010 Photovoltaics with piezoelectric core-shell nanowires *Nano Lett.* **10** 1108–12
- [67] Golam Sarwar A T M and Myers R C 2012 Exploiting piezoelectric charge for high performance graded InGa<sub>N</sub> nanowire solar cells *Appl. Phys. Lett.* **101** 143905
- [68] Pan C, Guo W, Dong L, Zhu G and Wang Z L 2012 Optical Fiber-based core-shell coaxially structured hybrid cells for self-powered nanosystems *Adv. Mater.* **24** 3356–61
- [69] Pan C, Niu S, Ding Y, Dong L, Yu R, Liu Y, Zhu G and Wang Z L 2012 Enhanced Cu(2)S/CdS coaxial nanowire solar cells by piezo-phototronic effect *Nano Lett.* **12** 3302–7

- [70] Sharma B K, Khare N and Ahmad S 2009 A ZnO/PEDOT:PSS based inorganic/organic heterojunction *Solid State Commun.* **149** 771–4
- [71] Wen X, Wu W and Wang Z L 2013 Effective piezo-phototronic enhancement of solar cell performance by tuning material properties *Nano Energy* **2** 1093–100
- [72] Wang Z, Qi J, Yan X, Zhang Q, Wang Q, Lu S, Lin P, Liao Q, Zhang Z and Zhang Y 2013 A self-powered strain sensor based on a ZnO/PEDOT:PSS hybrid structure *RSC Adv.* **3** 17011
- [73] Shoaee S, Briscoe J, Durrant J R and Dunn S 2014 Acoustic enhancement of polymer/ZnO nanorod photovoltaic device performance *Adv. Mater.* **26** 263–8
- [74] Shi J, Zhao P and Wang X 2013 Piezoelectric-polarization-enhanced photovoltaic performance in depleted-heterojunction quantum-dot solar cells *Adv. Mater.* **25** 916–21
- [75] Tang H, Liu B and Wang T 2015 Influence of piezoelectric fields on InGaN based intermediate band solar cells *J. Phys. D: Appl. Phys.* **48** 025101
- [76] Burschka J, Pellet N, Moon S-J, Humphry-Baker R, Gao P, Nazeeruddin M K and Gratzel M 2013 Sequential deposition as a route to high-performance perovskite-sensitized solar cells *Nature* **499** 316–9
- [77] Wang X, Li Z, Xu W, Kulkarni S A, Batabyal S K, Zhang S, Cao A and Wong L H 2015 TiO<sub>2</sub> nanotube arrays based flexible perovskite solar cells with transparent carbon nanotube electrode *Nano Energy* **11** 728–35
- [78] Hu G, Guo W, Yu R, Yang X, Zhou R, Pan C and Wang Z L 2016 Enhanced performances of flexible ZnO/perovskite solar cells by piezo-phototronic effect *Nano Energy* **23** 27–33